



HAL
open science

Impact of support oxide and Ba loading on the NO_x storage properties of Pt/Ba/support catalysts. CO₂ and H₂O effects.

E.C. Corbos, Xavier Courtois, Nicolas Bion, Patrice Marecot, Daniel Duprez

► To cite this version:

E.C. Corbos, Xavier Courtois, Nicolas Bion, Patrice Marecot, Daniel Duprez. Impact of support oxide and Ba loading on the NO_x storage properties of Pt/Ba/support catalysts. CO₂ and H₂O effects.. Applied Catalysis B: Environmental, 2007, 76 (3-4), pp.357-367. 10.1016/j.apcatb.2007.06.009 . hal-00300250

HAL Id: hal-00300250

<https://hal.science/hal-00300250>

Submitted on 27 Jan 2021

HAL is a multi-disciplinary open access archive for the deposit and dissemination of scientific research documents, whether they are published or not. The documents may come from teaching and research institutions in France or abroad, or from public or private research centers.

L'archive ouverte pluridisciplinaire **HAL**, est destinée au dépôt et à la diffusion de documents scientifiques de niveau recherche, publiés ou non, émanant des établissements d'enseignement et de recherche français ou étrangers, des laboratoires publics ou privés.

Impact of support oxide and Ba loading on the NO_x storage properties of Pt/Ba/support catalysts. CO₂ and H₂O effects.

E.C. Corbos, X. Courtois, N. Bion, P. Marecot, D. Duprez

Laboratoire de Catalyse en Chimie Organique, UMR 6503 CNRS, Université de Poitiers, 40 avenue du Recteur Pineau, 86022 Poitiers Cedex, France

Abstract

A series of 1wt%Pt/xBa/Support (Support = Al₂O₃, SiO₂, Al₂O₃-5.5wt%SiO₂ and Ce_{0.7}Zr_{0.3}O₂, x = 5-30wt% BaO) catalysts was investigated regarding the influence of the support oxide on Ba properties for the rapid NO_x trapping (100s). Catalysts were treated at 700°C under wet oxidizing atmosphere. The nature of the support oxide and the Ba loading influenced the Pt-Ba proximity, the Ba dispersion and then the surface basicity of the catalysts estimated by CO₂-TPD. At high temperature (400°C) in the absence of CO₂ and H₂O the NO_x storage capacity increased with the catalyst basicity: Pt/20Ba/Si < Pt/20Ba/Al5.5Si < Pt/10Ba/Al < Pt/5Ba/CeZr < Pt/30Ba/Al5.5Si < Pt/20Ba/Al < Pt/10BaCeZr. Addition of CO₂ decreased catalyst performances. The inhibiting effect of CO₂ on the NO_x uptake increased generally with both the catalyst basicity and the storage temperature. Water negatively affected the NO_x storage capacity, this effect being higher on alumina containing catalysts than on ceria-zirconia samples. When both CO₂ and H₂O were present in the inlet gas, a cumulative effect was observed at low temperatures (200°C and 300°C) whereas mainly CO₂ was responsible for the loss of NO_x storage capacity at 400°C. Finally, under realistic conditions (H₂O and CO₂) the Pt/20Ba/Al5.5Si catalyst showed the best performances for the rapid NO_x uptake in the 200-400°C temperature range. It resulted mainly from: (i) enhanced dispersions of platinum and barium on the alumina-silica support, (ii) a high Pt-Ba proximity and (iii) a low basicity of the catalyst which limits the CO₂ competition for the storage sites.

Keywords: NO_x storage; basicity; barium; alumina; silica; alumina-silica; ceria-zirconia.

1. Introduction

Exhaust gases from automotive engines have a marked impact on the air quality and the human health, especially in urban areas with high traffic density. In order to reduce this impact, more and more stringent regulations are imposed to automotive manufacturers. Diesel and direct injection gasoline engines have a potential for improving fuel efficiency and so to reduce CO₂ emissions. However, as they operate under an excess of oxygen (lean conditions), it is difficult to reduce nitrogen oxides. A promising solution to overcome this issue was introduced in the mid 1990s by Toyota with the concept of NO_x storage-reduction (NSR) [1]. This system is working under transient conditions. During the lean periods NO is oxidized into NO₂ over precious metals and trapped on a storage material, mainly as nitrates. Then, the engine switch to rich conditions (excess of hydrocarbons) for a short period allows one to release and to reduce stored NO_x.

Typically, NSR systems contain: (i) a high surface area support (e.g. Al₂O₃), (ii) a storage material (alkaline or alkaline earth oxides, e.g. BaO) and (iii) a component for NO_x oxidation/reduction (precious metals, e.g. Pt) [2]. The typical Pt/Ba/Al₂O₃ catalyst has been extensively studied during the last 10 years and several mechanisms were proposed for NO_x storage-reduction [3-12,15]. It is generally admitted in the literature that the NO_x storage takes place on multiple types of barium sites which have different activities toward NO_x adsorption [3,15], with the barium sites located in platinum proximity being the most active [3-5,12,15]. Barium can be present in the catalyst as BaO, Ba(OH)₂ and BaCO₃, depending on the reaction conditions [16], the NO_x storage occurring more preferentially on BaO than on Ba(OH)₂ followed by BaCO₃ [6]. The NO_x storage also depends on the reaction temperature [3,4,6], and presents a volcano type curve with an optimum near 350-380°C. Recently, it has been shown that after exposure to CO₂, Ba-containing species were roughly present in the catalyst under two main carbonate forms characterized by their thermal stability: low temperature (LT-BaCO₃) and high temperature (HTBaCO₃) species [13]. The well dispersed LT-BaCO₃ sites on the alumina support had a lower thermal stability and showed a higher activity toward NO_x storage-reduction than the bulk-like (HT-BaCO₃) sites. One of the main challenges would be to improve Ba dispersion in order to obtain catalysts which contain only the well dispersed barium sites which are responsible for a high NO_x storage capacity. Piacentini et al. [17] showed that the distribution of LT and HT-BaCO₃ species depends on both the chemical and textural properties of the support oxide and the Ba loading. Some studies have reported the role of the support oxide in the NO_x storage-reduction process [17-20]. Ce-Zr oxides, widely used in three way catalysts (TWC), were shown to be able to store NO_x and present improved sulfur tolerance [18-22]. Liotta et al. [20] proposed a Ce-Zr-Ba-Al₂O₃ catalyst as an improved material

to develop advanced NSR catalysts. Piacentini et al. [17], also found that for a same loading, Ba supported on ZrO₂ material had a NO_x storage capacity higher than on alumina until 27wt%Ba, and for low Ba loading (until 10 wt % Ba) CeO₂ supported catalysts presented the best properties. Contradictory results were obtained by Mathew et al. [23] who showed that Ba deposited on ceria-zirconia or zirconia oxides presented lower NO_x storage than on alumina. On the other hand, Eguchi and coll. [24] have studied MnO-ZrO₂ and Pt-ZrO₂-Al₂O₃ systems in dynamic conditions, and found that zirconia was basic enough to form stable nitrates on the surface whereas the carbonates were not produced.

Most studies reported in the literature were performed under unrealistic conditions, i.e. in the absence of H₂O and CO₂, these compounds being always present in the exhaust gas in a large proportion (10 vol. %). Moreover, the catalysts used to be activated under dry air and/or reduced under hydrogen in the 500-600°C temperature range. Nevertheless, some studies have reported that CO₂ had an important negative impact on the NO_x storage capacity due to the CO₂/NO₂ competition for adsorption on the storage sites [6,7,9,25-27] whereas it had a promoting effect on the NO_x release in the rich phase [28]. In the presence of CO₂, only surface barium nitrates were formed even if the storage was performed for a long time [7,25]. Water also negatively affected NO_x storage, mainly at low temperatures (200, 300°C) [6,9,25,27,29-31].

The aim of this work was to examine the effect of the support oxide (Al₂O₃, SiO₂, Al₂O₃5.5SiO₂ and Ce_{0.7}Zr_{0.3}O₂) and the Ba content (5-30wt%BaO) on the NO_x storage properties of Ba containing materials after hydrothermal oxidizing treatment at 700°C. The influence of CO₂ and H₂O on the NO_x storage capacity (rapid NO_x uptake) of the different catalysts was systematically investigated to get an in-depth view of catalyst NO_x storage performances under realistic conditions.

2 Experimental

Catalyst preparation

Four oxides were studied: (γ)-Al₂O₃ (Al), SiO₂ (Si), Al₂O₃-5.5 % SiO₂ (Al5.5Si) and Ce_{0.7}Zr_{0.3}O₂ (CeZr) as barium support for NO_x traps. The Pt/xBa/Support (where x is the loading in wt % of BaO and Support represents the support oxide) catalysts were prepared using the following method. The support was first calcined at 500°C for 4h under air and then impregnated with a barium nitrate solution, in order to obtain a 5, 10, 15, 20 or 30 wt % BaO content. After drying at 120°C for 12 hours, the barium containing support was calcined at 700°C (heating rate 5°C/min) under air for 4h. The resulting powder was then impregnated with a dinitro-diamino platinum

solution in order to obtain a 1 wt % Pt catalyst. After drying, the catalyst was calcined at 450°C under air for 2h and then activated at 700°C for 4h under a mixture containing 10 % O₂, 10 % H₂O, and N₂.

NO_x storage capacity measurements

Before the NO_x storage capacity measurements, the catalyst sample (60 mg) was pretreated at 550°C for 30 min under a 10 % O₂, 10 % H₂O, 10 % CO₂ and N₂ mixture (total flow rate: 10 L.h⁻¹) and cooled down to the storage temperature under the same mixture. The sample was then submitted to a 350 ppm NO, 10 % O₂, 10 % H₂O, 10 % CO₂ and N₂ mixture (total flow rate: 10 L.h⁻¹) at 200, 300 or 400°C. After the NO_x storage test, the catalyst was refreshed by elevating the temperature at 550°C under lean conditions which led to complete NO_x desorption. For the test performed without H₂O or CO₂ or both, the catalysts were pretreated and cooled down to storage temperature under the same mixture used for the NO_x storage. For example, for the measurement of NO_x storage capacity at 300°C in the presence of CO₂ the catalysts were pretreated at 550°C and cooled down to 300°C under a mixture containing CO₂, O₂ and N₂. The gas flow was introduced using mass-flow controllers, except for H₂O vapors which were introduced using a saturator thermostated at 46°C. Both NO and NO_x concentrations (NO+NO₂) were followed by chemiluminescence with a COSMA Topaze 2020 apparatus. H₂O was removed prior to NO_x analysis with a membrane dryer. The NO_x storage capacity was estimated by the integration of the recorded profile for the first 100s and platinum oxidation activity was estimated at saturation (usually about 900s) as the NO₂/NO_x ratio (%). Under the conditions used in NO_x storage measurements (60 mg, 10 L.h⁻¹, 350 ppm NO) a maximum of 67 μmol NO_x per gram of catalyst can be stored. This corresponds to the complete trapping of NO_x injected on the catalyst in 100s.

Catalyst characterizations

X-ray powder diffraction was performed at room temperature with a Siemens D5005 BraggBrentano (θ-θ) apparatus using a Kα Cu radiation (λ=0.154056 nm). The diffractograms were recorded with a step of 0.02° 2θ, dwell time 2s. The powder was deposited on a silicium wafer. The crystalline phases were identified by comparison with the ICDD database files. The in-situ XRD measurements at different temperatures were carried out in an Anton PAAR HTK16 high temperature stainless chamber linked to a Siemens D8 (Bragg-Brentano θ-θ) powder diffractometer. The powders were supported on a Kanthal foil. The powders were heated under He from 25°C to 800°C with a heating rate of 10°C.min⁻¹. Diffractograms were recorded with an increment of

0.04° 2 θ and a dwell time of 2s. Quantitative analysis of crystalline BaCO₃ has been performed by XRD using full width at half maximum intensity of the peak for the (111) and (021) reflections with the Scherrer's equation: $d = (0.9 \cdot \lambda / \beta \cdot \cos\theta)$, in which β stands for the FWHM (full width at half maximum) intensity in radians (2 θ scale) and θ is the Bragg angle. The instrumental broadening was determined from the pattern of bulk LaB₆ standard.

The BET surface areas were deduced from N₂ adsorption at -196°C carried out with a Tristar 3000 Micromeritics apparatus. Prior to the measurement, the samples were pretreated at 350°C under vacuum for 12h in order to eliminate the adsorbed species. The pore distribution was determined from the desorption isotherm.

Transmission electron microscopy (TEM) images were obtained with a Philips CM 120 microscope operating at 120 kV, equipped with an energy-dispersive X-ray detector (EDX). The sample was suspended in ethanol and spread onto a copper grid covered with a thin layer of carbon. The noble metal dispersion of Pt-containing catalysts was determined by using the H₂ chemisorption method. The catalysts were first reduced under pure hydrogen at 500°C for 1h and then degassed at the same temperature under Ar for 3h. The reactor was cooled under Ar at room temperature, where hydrogen was dosed on the sample until saturation. For the ceria containing catalysts the chemisorption experiments were carried out at -85°C. This low temperature is necessary to avoid hydrogen spillover on ceria support [32]. After flushing under Ar for 10 min, the sample was exposed to hydrogen again. The amount of chemisorbed hydrogen was taken as the difference between the two hydrogen exposures.

The basicity of catalysts was estimated by thermal programmed desorption (TPD) of CO₂.

Before measurement, the catalysts were pre-treated at 550°C for 30 min under a 1 % O₂/He flow. Then, the catalysts were cooled down to 50°C, and the adsorption of CO₂ was carried out for 1h. After flushing under 1 % O₂/He mixture at 50°C to remove the physisorbed species, the CO₂ thermal desorption was followed by thermal conductivity from 50°C up to 700°C.

IR spectra were obtained with a Nicolet 5700 FT-IR apparatus. The spectra were collected in the range 1100-4000 cm⁻¹ with a resolution of 4 cm⁻¹ and a scan number of 64. The samples, in the form of self-supporting wafer (15-25 mg), have been activated at 500°C under secondary vacuum. Then the samples were taken at room temperature and exposed to CO₂ atmosphere. After flushing under nitrogen at the same temperature, IR spectra were obtained under secondary vacuum from room temperature until 500°C.

3. Results and discussion

3.1 Structural and morphological properties of the catalysts

BET and pore distribution

In order to gain information about the way that barium loading affects the structural properties of the different supports, the materials were characterized with respect to their specific surface area, pore volume and pore size distribution before and after barium impregnation and subsequent calcination at 700°C.

The BET surface areas of the support oxides were 144 m².g⁻¹, 147 m².g⁻¹, 317 m².g⁻¹, and 80 m².g⁻¹ for Al₂O₃, SiO₂, Al₂O₃-5.5 wt % Si and Ce_{0.7}Zr_{0.3}O₂, respectively. As shown in Fig. 1, Ba addition led to a decrease in surface area, this effect being more marked for the high barium loading whatever the support oxide. The cumulative pore volume (V_p) is also reported in the same figure. For the Ba/Si and Ba/Al_{5.5}Si materials, the evolution of the BET surface area is proportional to that of the pore volume as a function of the Ba loading (Fig. 1). This result indicates that the decrease of the BET surface was mainly due to the decrease of pore volume by plugging of a part of the pores with the Ba component, which is confirmed by the pore size distribution depicted in Fig. 2. Moreover, even at high loading, barium deposition did not lead to a significant change of the average pore diameter in the case of Si and Al_{5.5}Si supports indicating that Ba deposit is able to block all the pores whatever their size. On the other hand, for Ba/CeZr and Ba/Al materials, the BET surface area dropped at high Ba loading while the cumulative pore volume was slightly affected or even increased. As shown in Fig.2, this phenomenon resulted from both the blocking of small pores and the formation of larger ones. Consequently, the average pore diameter increased for the highest barium loading, from 11 nm to 18 nm for alumina supported barium and from 6 nm to 11 nm for ceria-zirconia supported barium. This result can be explained by the formation of cracks in the BaCO₃ layers giving rise to new larger pores [17] and/or by the formation of new phases [33]. After addition of platinum and subsequent thermal treatment at 700°C the different materials did not show significant modifications of the BET surface area except for the Pt/20Ba/Al and Pt/20Ba/Si samples (Table 1). In these latter cases, the loss of the BET surface area would result from the plugging of a part of the pores by the migration of some Ba during the impregnation step of platinum [33].

Table 1: BET surface area before and after Pt impregnation.

Support	Al			Si		Al5.5Si			CeZr		
BaO (wt %)	10	15	20	10	20	10	20	30	5	10	20
BET without Pt ($\text{m}^2 \cdot \text{g}^{-1}$)	131	120	93	120	96	319	200	160	62	47	30
BET with Pt ($\text{m}^2 \cdot \text{g}^{-1}$)	126	118	74	106	78	319	200	160	56	43	27

Table 2: BaCO_3 mean particle size deduced from XRD and main crystallized Ba containing phases present on the different catalysts.

Support	Al		Si		Al5.5Si		CeZr	
BaO (wt %)	10	20	10	20	20	30	5	10
Ba content ($\mu\text{mol} \cdot \text{m}^{-2}$)	5.19	17.7	6.17	16.8	6.54	12.3	5.84	15.2
BaCO_3 d(nm)	26	35	23	28	*	25	19	51
Other Ba containing phases	*	BaAl_2O_4	*	BaSiO_3	BaAl_2O_4	BaAl_2O_4	*	$\text{Ba}_2\text{CeZrO}_{5.5}$

* not mesurable

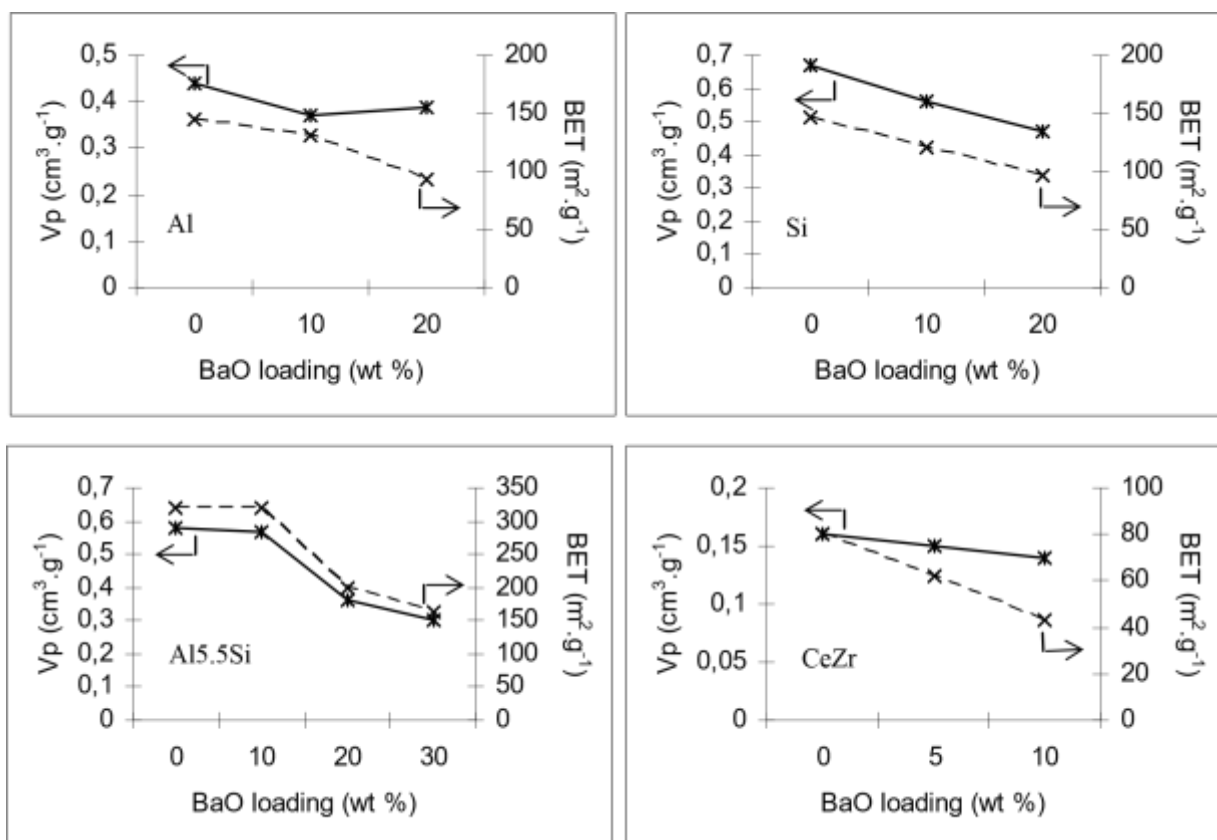


Figure 1: BET surface area (dotted black lines) and cumulative pore volume (continue lines) versus the Ba loading on different support oxides.

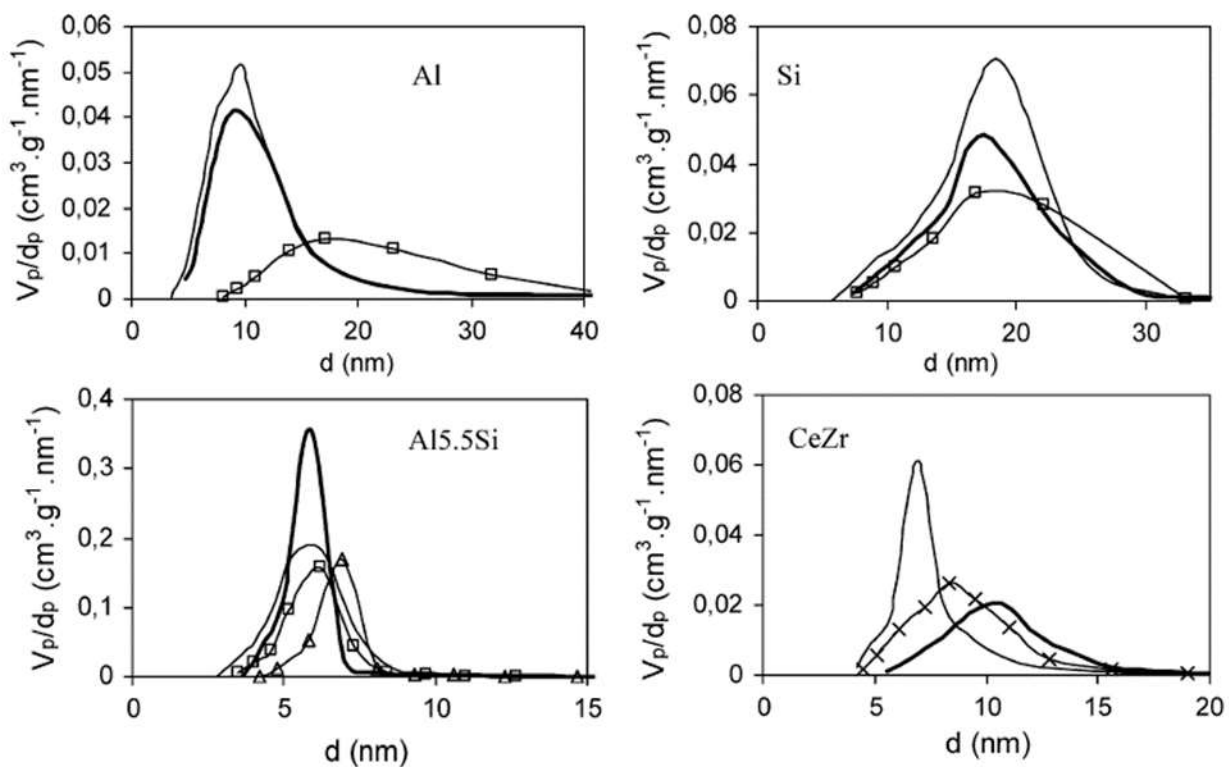


Figure 2: Pore size distribution of the supports and Ba/Support materials after calcination at 700°C. (—) 0BaO, (x) 5BaO (—) 10BaO, (□) 20BaO, (Δ) 30Ba

XRD measurements

The presence of different Ba-containing crystalline phases on the catalysts was investigated by XRD. X-ray diffraction patterns of the barium doped samples calcined at 700°C and then exposed to ambient atmosphere are shown in Fig. 3. The main crystalline phases present on the different catalysts and the BaCO_3 crystallite sizes estimated from XRD measurements are summarized in Table 2. The amount of Ba introduced by impregnation expressed in $\mu\text{mol Ba per m}^2$ are also reported in Table 2.

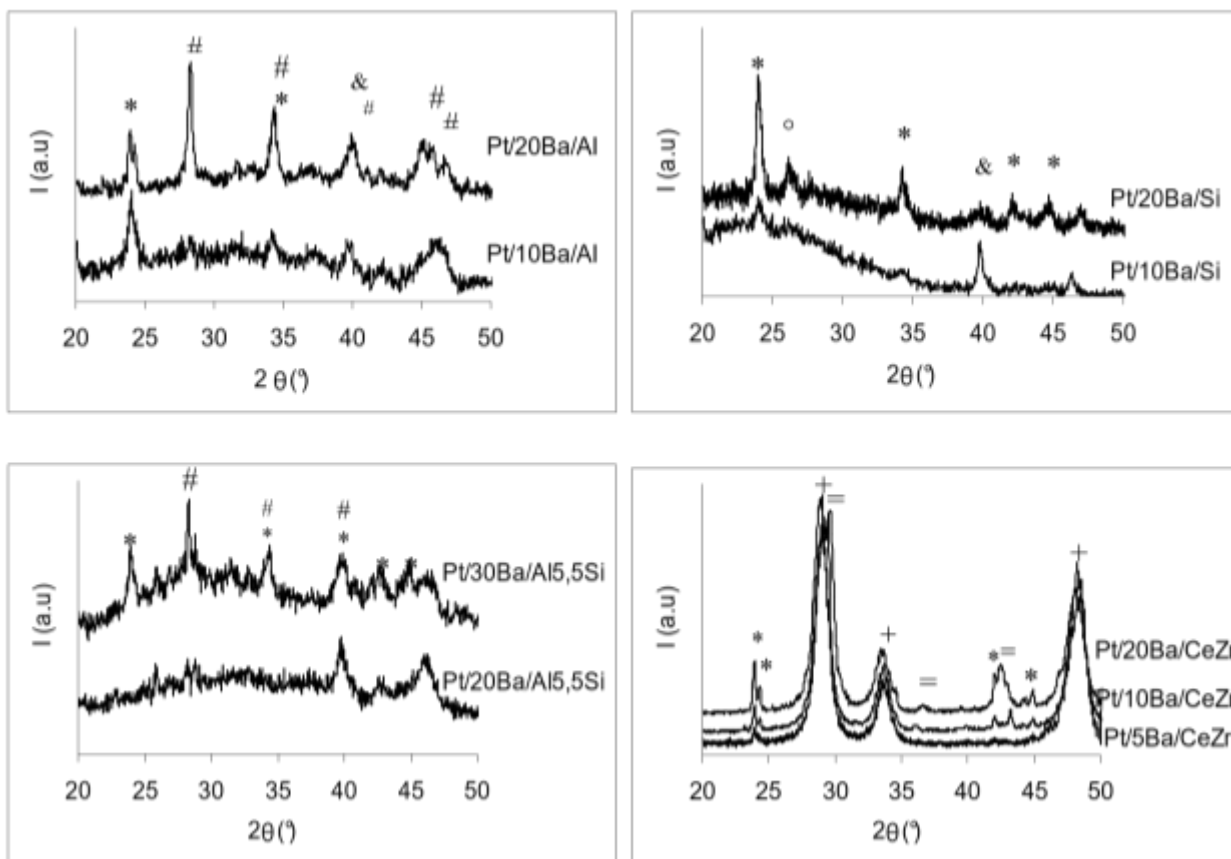


Figure 3: XRD patterns of the catalysts; (*) BaCO_3 , (#) BaAl_2O_4 , (&) Pt, (°) BaSiO_3 , (+) $\text{Ce}_{0.6}\text{Zr}_{0.4}\text{O}_2$, (=) $\text{Ba}_2\text{CeZrO}_{5.5}$.

The formation of orthorhombic barium carbonates (whiterite orthorhombic $2\theta = 23.9^\circ, 24.3^\circ$), even at low Ba content (10 wt % BaO), was observed on Al_2O_3 , SiO_2 and $\text{Ce}_{0.7}\text{Zr}_{0.3}\text{O}_2$ supported catalysts while on the $\text{Al}_2\text{O}_3\text{5.5SiO}_2$ supported catalyst, crystallized BaCO_3 was observed only for the 30 wt % catalyst. This result can be explained by the high surface area of the silica-alumina oxide compared to the other supports. However, when comparing the BaCO_3 crystallite size deduced from the XRD measurements, it is observed that the Pt/10Ba/Al, Pt/10Ba/Si and Pt/5Ba/CeZr catalysts present close values (26 nm, 23 nm and 19 nm, respectively) for similar $\text{Ba}\cdot\text{m}^{-2}$ values ($5.19, 6.17$ and $5.84 \mu\text{mol}\cdot\text{m}^{-2}$, respectively). On the other hand, for a $6.54 \mu\text{mol}\cdot\text{m}^{-2}$ value, BaCO_3 was not detected on the Pt/20Ba/Al5.5Si catalyst. In summary, the alumina-silica support would allow one to restrict the growth of the barium component. Otherwise, the mean Ba crystallite size deduced from XRD is higher than the mean pore size of the different support oxides, supporting the previous conclusion, i.e. the decrease of BET surface area resulted from the plugging of some pores by the Ba component.

Recently, Piacentini et al. [17] reported that crystallized BaCO₃ (orthorhombic and monoclinic) was formed on silica support only for high Ba loadings (28 wt % Ba) while on alumina support, Ba-containing phases were amorphous until 16.7 wt % Ba content. In our study, crystalline BaCO₃ was observed even at low Ba loading (10 wt % BaO) for both supports. The difference may come from the fact that we exposed our catalysts to CO₂ from ambient air while Piacentini et al. carried out their study in-situ where carbonates resulted only from the decomposition of Ba(C₂H₃O₂)₂. Moreover, as we treated our catalysts at 700°C under O₂, H₂O and N₂, we can expect that during the thermal treatment Ba particles sintered, leading to larger Ba particles.

Increasing Ba loading led to the apparition of new diffraction peaks corresponding to different barium containing phases depending on the support oxide: BaAl₂O₄ on the Pt/20Ba/Al, Pt/20Ba/Al5.5Si and Pt/30Ba/Al5.5Si materials, BaSiO₃ on the Pt/20BaSi catalyst and Ba₂CeZrO_{5.5} for 10 and 20 wt % BaO on the ceria-zirconia mixed oxide [17,35-37]. The presence of these phases for lower BaO contents may not be excluded, if their size is under the detection limit and/or the quantity is very small.

TEM coupled to EDX-analysis

An important parameter in the NO_x storage-reduction process is the Pt-Ba proximity [312,15]. In order to gain information about Pt-Ba proximity, catalysts were characterized by transmission electron microscopy (TEM) coupled with X-analysis. Representative micrographs of the Pt/20Ba/Si and Pt/20Ba/Al5.5Si catalysts are depicted in Fig. 4. For the Pt/20Ba/Si material, EDX revealed no proximity between Pt particles and the Ba component (Fig. 4a). Conversely, barium was always detected in the neighboring of platinum on the Pt/20Ba/Al5.5Si catalyst. An intermediate behavior was observed for the Pt/20Ba/Al and Pt/10BaCeZr materials with platinum deposited on both the Ba component and the support oxide (micrographs not shown). Moreover, Fig. 4 shows that platinum particle size is lower on the Pt/20Ba/Al5.5Si catalyst than on the Pt/20Ba/Si (5-10 nm and 20-30 nm, respectively). These differences were also confirmed by H₂ chemisorption experiments (Table 3).

Table 3: Platinum dispersion and mean particle size determined with H₂ chemisorption.

Support	Al		Si		Al5.5Si			CeZr	
BaO (wt %)	10	20	10	20	10	20	30	5	10
D (%)	7	5	4	3	9	12	10	10	6
\overline{d} (nm)	15	22	25	33	11	8	11	10	16

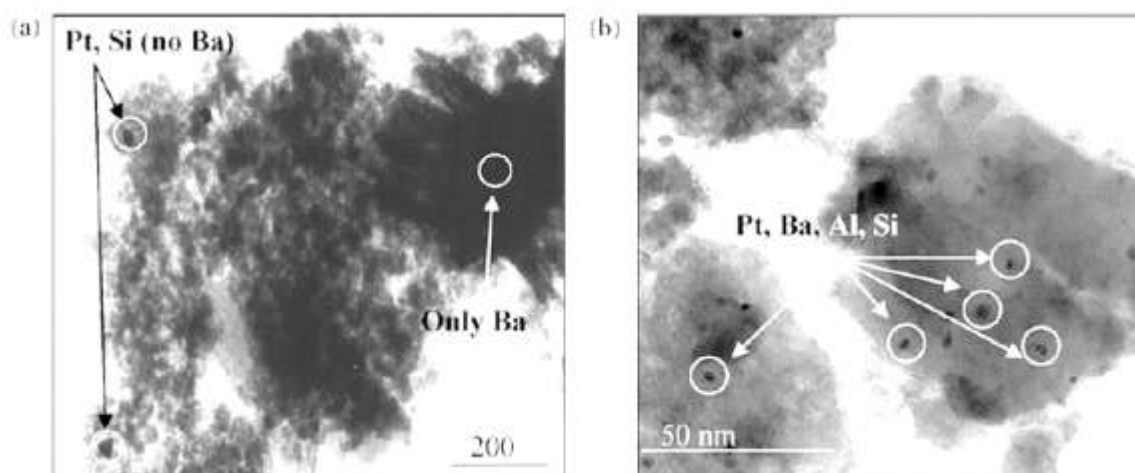


Figure 4: Micrographs of (a) Pt/20Ba/Si and (b) Pt/20Ba/Al_{5.5}Si catalysts.

3.2 Basicity measurements

Catalyst basicity was estimated by thermodesorption of CO₂ in a 1 % O₂/He atmosphere after thermal treatment of the sample at 550°C in 1 % O₂/He and subsequent exposure to CO₂ at 50°C for 1h. Fig. 5 shows CO₂ evolution traces recorded during heating various catalyst samples in 1 % O₂/He from 50°C to 700°C. In parallel, a similar protocol was performed into an IR cell in order to determine by FTIR spectroscopy the nature of the CO₂ adsorbed species which desorb in the 50°C-500°C temperature range. The CO₂ desorption peak observed by TPD at low temperature around 100°C matches well with the disappearance of the bands characteristic to the vibrations of the hydrogen carbonate species HO-CO₂⁻ ($\nu(\text{OH}) \approx 3610 \text{ cm}^{-1}$ and $\delta(\text{OH}) \approx 1230 \text{ cm}^{-1}$, spectra not shown). In the 150°C - 550°C temperature range, a more or less significant desorption of CO₂ depending on catalyst composition (Fig. 5). The wavenumbers of the bands which the intensities decrease in this temperature range differ from the oxide support. However, for each support, one can assign the bands observed to carbonate species differently coordinated on the barium. Moreover on the basis of the splitting of the asymmetric stretching ν_3 vibration, we can distinguish that unidentate and bidentate barium carbonate species are progressively decomposed up to 450°C except on the Pt/10Ba/CeZr where some bidentate species remain at this temperature. Above this temperature only one wide band at around 1450 cm⁻¹ is still present on the FTIR spectra. This feature can be assigned to polydentate barium carbonate species similar to bulk carbonates or well crystallized BaCO₃ (pure BaCO₃ giving the same band). These last species can be responsible for the broad CO₂ peak at high temperature on TPD curves. Generally, the intensity of this peak increases with the Ba content of the material whatever the oxide support. In order to corroborate the identification of the carbonates responsible for the CO₂ desorption in the 500°C – 700°C

temperature range, BaCO_3 decomposition was followed by XRD. The experiments were performed in situ under He flow and XRD spectra were obtained at different temperatures between room temperature and 800°C . For this purpose, the Pt/20Ba/Al, Pt/30Ba/Al5.5Si and Pt/10Ba/CeZr catalysts which present a well-defined BaCO_3 diffraction peak were chosen. The relative evolutions of the main BaCO_3 diffraction peak are reported in Fig. 6. It can be observed that the intensity of the BaCO_3 diffraction peak starts decreasing from 450°C - 500°C and the temperature at which the total decomposition of BaCO_3 is achieved depends on the nature of the support oxide. For the Al5.5Si and Al supported catalysts the BaCO_3 decomposition is completed at 700°C and 750°C , respectively, while on the CeZr supported catalyst crystallized BaCO_3 can be observed even after heating at 800°C . This result can partially be explained by the mean BaCO_3 particle size which increased following the order: Pt/30Ba/Al5.5Si (25 nm) < Pt/20Ba/Al (35 nm) < Pt/10Ba/CeZr (51 nm). Thus, the higher the BaCO_3 crystallite size, the higher the temperature of BaCO_3 decomposition. Otherwise, it must be recalled that these decomposition temperatures are much lower than that of the bulk- BaCO_3 ($> 900^\circ\text{C}$) [38]. No BaO formation was detected during the experiments, indicating that the BaCO_3 decomposition was probably accompanied by the reaction of BaO with the support oxide resulting in the formation of new phases as reported in Table 2.

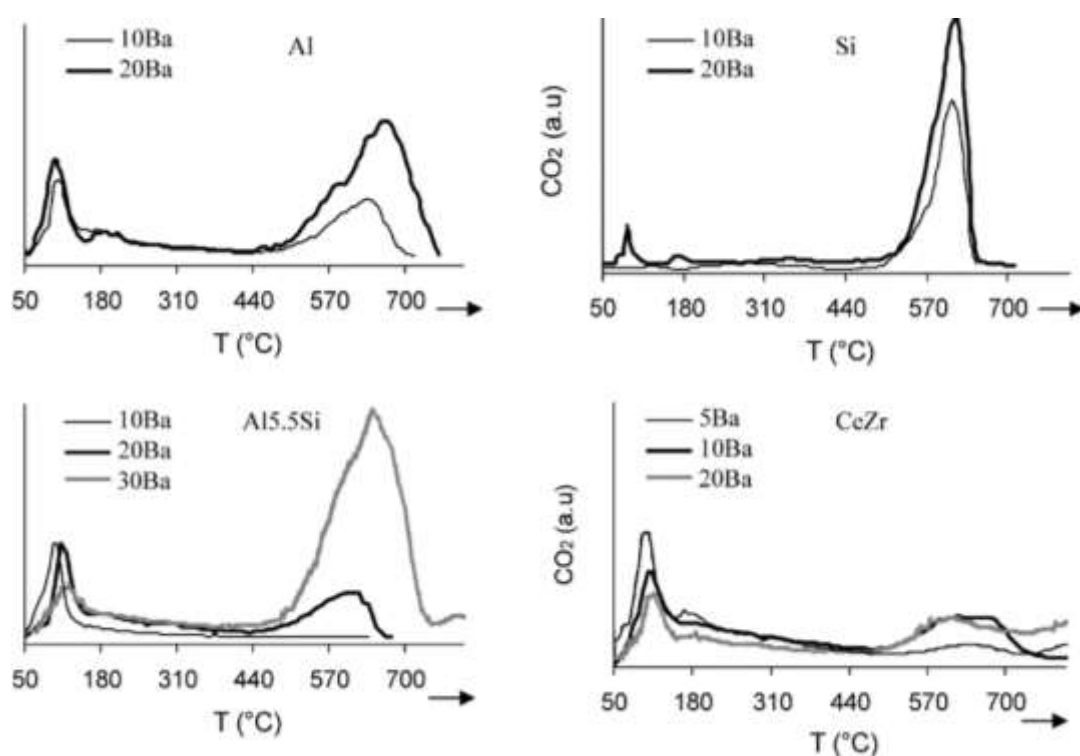


Figure 5: CO_2 - TPD profiles of different catalysts after adsorption of CO_2 at 50°C . Before CO_2 adsorption the catalysts were pretreated at 550°C under 1% O_2 for 30min.

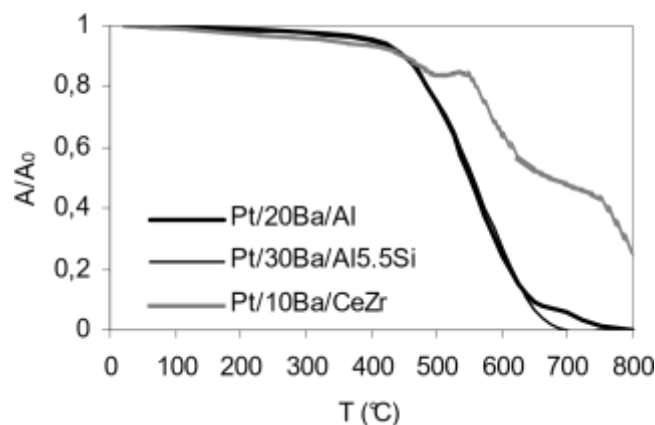


Figure 6: Relative area (peak area at temperature T/initial peak area) for (111) reflection peak of BaCO₃.

In summary, the broad CO₂ desorption peak observed in the 500°C - 700°C temperature range corresponds to the decomposition of more or less crystallized BaCO₃. In order to check if a part of these barium species contributes to the NO_x storage, the carbonated Pt/10Ba/CeZr catalyst was submitted to NO_x storage at 400°C after thermal treatment under 10 % O₂/N₂ at increasing temperature from 400°C to 700°C. The NO_x storage experiments were performed without water and CO₂ in the inlet gas. The values reported in Table 4 show that the NO_x storage capacity increases with the temperature of the treatment until 550°C and then remains constant for the higher temperatures. This result can be explained by assuming that some barium sites which desorb CO₂ until 550°C can participate to NO_x storage at 400°C. This is not the case for the Ba sites involved in the CO₂ desorption at higher temperature (> 550°C) that would correspond only to bulk Ba containing phases. Consequently we estimated the surface basicity of the different materials by the amount of CO₂ desorbed between 150°C and 550°C. The values reported in Table 5 show that the basicity of the catalysts increases with the Ba content whatever the support oxide. Moreover, concerning the effect of the oxide component for a same Ba loading, the basicity decreases following the sequence Pt/Ba/CeZr > Pt/Ba/Al > Pt/Ba/Al5.5Si > Pt/Ba/Si.

Table 4: NO_x storage capacity at 400°C of the Pt/10Ba/CeZr catalyst. Before measurements, the catalyst was pre-treated at 400, 500°C, 550°C, 600°C or 700°C.

Pre-treatment	400°C	500°C	550°C	600°C	700°C
NO _x stored (μmol.g ⁻¹)	41.8	47.8	51.3	51.4	51.4
NO ₂ /NO _x (%)	34	38	39	39	38

Table 5: Amount of CO₂ (μmol.g⁻¹) desorbed during CO₂-TPD experiments from 150°C to 550°C as a function of Ba loading and support oxide.

Support	Al		Si		Al5.5Si		CeZr	
BaO (wt %)	10	20	10	20	20	30	5	10
CO ₂ (μmol.g ⁻¹)	105	134	42	85	108	128	125	169

3.3 NO_x storage capacity

The different catalysts were tested for their behavior in NO_x storage at 200°C, 300°C and 400°C under the conditions described in the experimental part. A high space velocity was chosen in order to store between 10 % and 80 % of the inlet NO_x during the first 100s. First, the tests were performed in the absence of water and CO₂ in the gas feed, then with 10 % H₂O or 10 % CO₂ and finally with both water and CO₂.

Absence of H₂O and CO₂

The pretreated catalysts were exposed to the NO_x containing mixture for 900s. Data reported in Fig. 7 correspond to the amount of NO_x (μmol.g⁻¹) stored during the first 100s. The NO oxidation efficiencies (NO₂/NO_x, %) listed in Table 6 were determined at the end of the storage cycle (900s). Figure 7 shows that the NO_x storage capacity depends on both the reaction temperature and the catalyst composition. It increases with the storage temperature for the Pt/20Ba/Al, Pt/30Ba/Al5.5Si, Pt/5Ba/CeZr and Pt/10Ba/CeZr catalysts. The reverse evolution is observed for the Pt/20Ba/Al5.5Si catalyst while the NO_x storage is nearly independent of the temperature for the Pt/10Ba/Al and Pt/20Ba/Si materials.

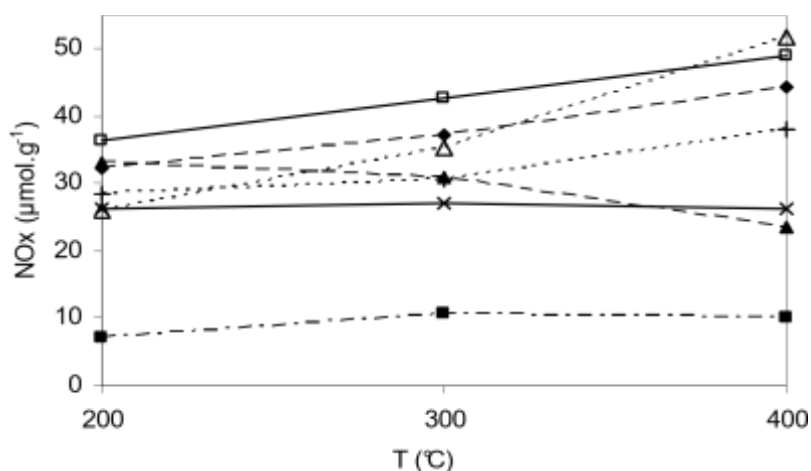


Figure 7: NO_x storage capacity of the catalysts measured without water and CO₂ in the inlet gas at 200, 300 and 400°C; (x) Pt/10Ba/Al, (■) Pt/20Ba/Si, (□) Pt/20Ba/Al, (▲) Pt/20Ba/Al5.5Si, (◆) Pt/30Ba/Al5.5Si, (+) Pt/5Ba/CeZr, (Δ) Pt/10Ba/CeZr.

Table 6: NO₂/NO_x ratio (%) determined at 900s under different gas mixtures at 200°C, 300°C and 400°C.

Reaction mixture Catalyst / T (°C)	Without H ₂ O and CO ₂			With H ₂ O			With CO ₂			With H ₂ O and CO ₂		
	200	300	400	200	300	400	200	300	400	200	300	400
Pt/10Ba/Al	17	32	36	11	23	29	17	34	40	10	24	30
Pt/20Ba/Al	22	40	45	13	30	38	23	44	46	12	20	38
Pt/20Ba/Al5.5Si	19	42	48	8	29	37	18	38	43	9	29	36
Pt/30Ba/Al5.5Si	10	26	36	4	14	26	10	25	34	13	21	30
Pt/5Ba/CeZr	9	12	27	7	11	25	8	13	25	7	12	24
Pt/10Ba/CeZr	5	7	39	7	7	24	6	7	22	6	7	18
Pt/20Ba/Si	20	30	36	10	21	25	-	-	36	10	20	26

Many works [3,4,39] in the literature have reported a maximum NO_x storage occurring between 350°C and 400°C on Pt/BaO/Al₂O₃ catalysts in a feed containing NO and O₂. It was shown that the temperature giving the maximum NO_x uptake was a function of the storage time and the initial state of the catalyst [2]. At lower temperatures NO oxidation is typically considered as the main rate limiting step for the overall NO_x storage trapping process [2]. On the other hand, the decrease in trapping capacity at high temperatures is mainly caused by the decreasing thermodynamic stability of nitrate species [40,41], even though the thermodynamic limitation in NO oxidation encountered at temperatures exceeding 300°C may also play a role. In the present work, the correlation obtained by reporting the NO_x storage capacity measured at 400°C as a function of catalyst basicity evaluated by CO₂-TPD shows that the storage capacity increases with the basicity of the materials (Fig. 8). This result confirms that the main limiting parameter for the NO_x storage at high temperature is nitrate stability.

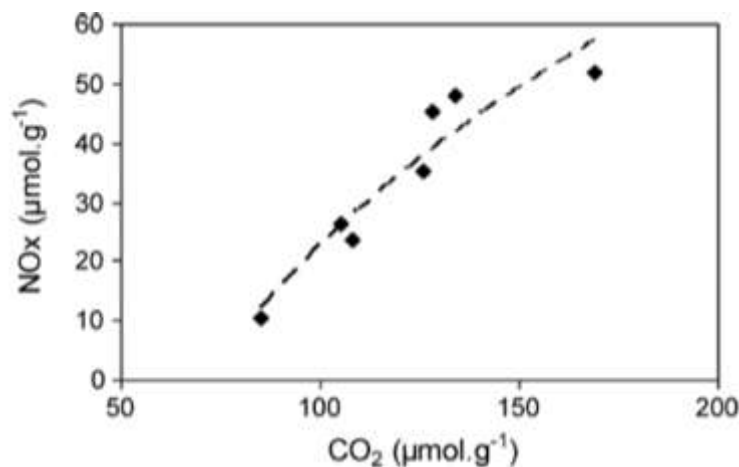


Figure 8: NO_x storage capacity at 400°C for the first 100s as a function of CO₂ desorbed from 150 to 550°C.

Concerning the NO_x storage experiments performed at 200°C, Fig. 7 and Table 6 show that the NO_x storage capacities are not directly linked to the NO oxidation in NO₂. For example, the Pt/20Ba/Al and Pt/20Ba/Si catalysts, which present similar oxidation activities (NO₂/NO_x = 22 % and 20 %, respectively), exhibit the highest and the lowest storage capacities, respectively (stored NO_x = 36.4 μmol.g⁻¹ versus 7.1 μmol.g⁻¹). Consequently, other parameters must be taken into consideration to explain the NO_x storage data obtained at 200°C. Thus, the low performance of the Pt/20Ba/Si catalyst may result partly from its weak basicity. Nevertheless, the Pt/20Ba/Al5.5Si catalyst which is one of the less basic materials tested in this work (108 μmol.g⁻¹ CO₂) was able to store NO_x at 200°C practically as the Pt/20Ba/Al sample which was the most active for the NO_x storage at this temperature (36.4 μmol.g⁻¹). Otherwise they had similar oxidation activities (NO₂/NO_x = 19 and 22 %, respectively). Another important parameter involved in the literature for the NO_x storage is the Pt-Ba proximity [3-5,12,15]. Many works [3-5,12,15], reported that Ba sites in contact with Pt particles or in their close proximity were likely the sites responsible for the rapid uptake of NO_x. TEM characterization coupled to EDX described in a former section, have shown significant differences in platinum distribution at the catalyst surface as a function of the support oxide. For example, no Pt-Ba interactions have been observed on the Pt/20Ba/Si catalyst while the EDX analysis has revealed that platinum was mainly present in the close proximity of the Ba component on the Pt/20Ba/Al5.5Si catalyst. These observations allowed one to account for the high NO_x storage capacity measured at 200°C on the Pt/20Ba/Al5.5Si (33.0 μmol.g⁻¹) sample in comparison with that on the Pt/20Ba/Si material which is very low (7.1 μmol.g⁻¹). Note that contrary to silica oxide, the alumina containing supports can contribute to NO_x storage at low temperature (200-300°C) [25,27,29,39,42]. It is expected that this contribution will decrease at higher barium loadings.

Otherwise, the Pt/10Ba/CeZr catalyst exhibited a significant NO_x storage capacity at 200°C in spite of a very poor oxidation activity (NO₂/NO_x = 5 %). This result suggests that NO_x storage at 200°C would not proceed through the oxidation of NO to NO₂ followed by the adsorption of NO₂ on the storage material. In accordance with previous work [3-6] reporting that the NO_x storage below 300°C can occur through NO adsorption as nitrites, we suggest the following reaction for NO_x storage at 200°C on the Pt/10Ba/CeZr catalyst: $\text{BaO} + 2\text{NO} + \text{O}^* = \text{Ba}(\text{NO}_2)_2$ where O* would originate from the dissociative adsorption of O₂ on platinum in close proximity of the Ba component or from ceria oxide.

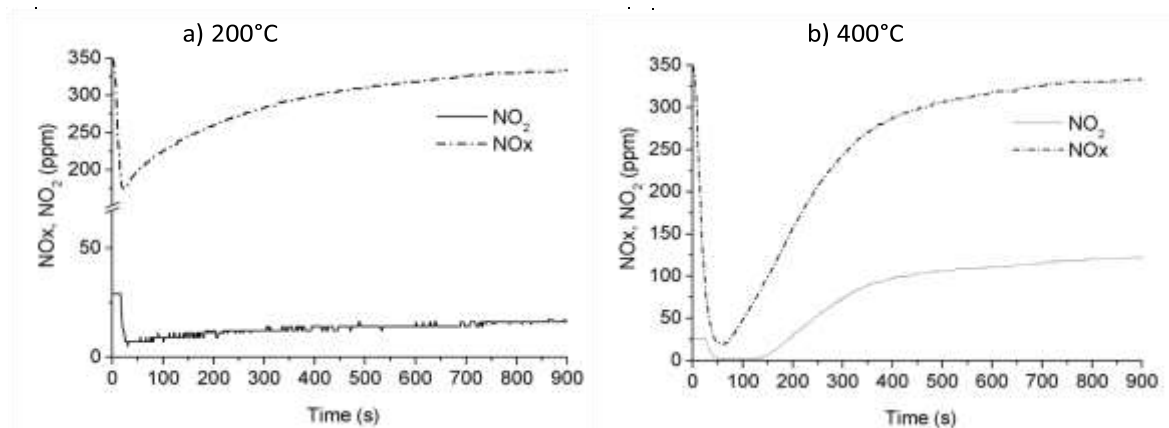


Figure 9: NO_x and NO₂ outlet curves for Pt/10Ba/CeZr catalyst obtained during NO_x storage capacity measurements without H₂O and CO₂ (a) at 200°C and (b) at 400°C.

The NO₂ reactor outlet concentrations depicted in Fig. 9 tend to confirm the NO_x storage as nitrites. Indeed, no NO₂ consumption was observed during the initial storage phase at 200°C. The slight increase of the NO₂ concentration as a function of time may result from a decrease of the basic character of the Ba component after NO_x adsorption (Fig. 9a). As a consequence, the Pt oxides in interaction with Ba would be less stable, i.e. more reactive for NO oxidation [43]. On the other hand, Fig. 9b shows that NO₂ produced during the initial step of storage at 400°C (≈100s) was totally consumed and then the NO₂ trace increased to reach a nearly constant level at 900s. This behavior proves that NO₂ plays a prominent role in NO_x storage at 400°C. The NO_x trapping at this temperature would mainly occur through the oxidation of NO into NO₂ on platinum particles followed by the adsorption on storage sites [2 and associated references].

Presence of CO₂ or H₂O

Previous works [6,7,9,25-27,29-31] have demonstrated the harmful effect of CO₂ and (or) H₂O on the performances of NSR catalysts. However, the investigations were generally achieved on a single model Pt/Ba/Al₂O₃ catalyst up to saturation by NO_x. The aim of the present study was to examine the effect of CO₂ and H₂O on the rapid NO_x trapping at different temperatures for catalysts differentiated by their Ba loading and support oxide. The loss of NO_x storage capacity (expressed in %) due to the presence of CO₂, H₂O or both are reported in Table 7.

Table 7: Loss of NO_x storage capacity (%) due to the presence of CO₂ and H₂O for different catalysts.

NO _x storage loss (%)		With CO ₂			With H ₂ O			With H ₂ O and CO ₂		
Catalyst	/ T (°C)	200	300	400	200	300	400	200	300	400
Pt10BaAl		8	16	31	24	25	7	50	49	30
Pt20BaAl		30	44	59	20	22	31	59	61	60
Pt20BaAl5.5Si		9	9	25	33	15	0	40	15	7
Pt30BaAl5.5Si		31	45	59	23	21	30	56	50	53
Pt5BaCeZr		37	41	42	21	18	13	68	60	50
Pt10BaCeZr		67	66	58	3	2	11	64	68	58

It clearly appears an inhibiting effect of CO₂ for NO_x trapping on the various materials. Nevertheless, the CO₂ effect depends on the catalyst composition and the temperature of the storage test. On alumina and silica-alumina supported catalysts the detrimental effect of CO₂ increases with both the Ba loading and the storage temperature. On the other hand, the inhibiting effect of CO₂ observed on ceria-zirconia catalysts does not depend significantly on the temperature of the run, with a drop of 60-70 % for the Pt/10Ba/CeZr and 40 % for the Pt/5Ba/CeZr whatever the reaction temperature. In previous works [7,9], the increased CO₂ inhibitor effect with the storage temperature was generally attributed to the increased barium carbonate stability in the presence of CO₂ compared to the respective nitrates. The NO₂/NO_x data reported in Table 6 show that CO₂ has practically no influence on the oxidation activity of the catalysts whatever the support oxide and the Ba loading. Such an observation suggests that the inhibiting effect of CO₂ results only from the competition between CO₂ and NO_x for the adsorption sites on the storage material [6,7,9,25]. When comparing the loss of NO_x storage capacity due to the presence of CO₂ and the catalyst basicity obtained by CO₂-TPD (Fig. 10), it appears that the inhibiting effect of CO₂ for NO_x adsorption is generally more significant for the catalysts showing a high basicity whatever the storage temperature.

As a consequence, the NO_x storage capacities measured at 400°C on the different materials in the presence of CO₂ are relatively close (Table 8), except for the silica supported sample which has a very low storage capacity (8 μmol.g⁻¹). Moreover, the Pt/20Ba/Al5.5Si catalyst, which is one of the less basic materials studied in this work, becomes the most active at 200°C and 300°C for NO_x trapping in a CO₂ containing feed.

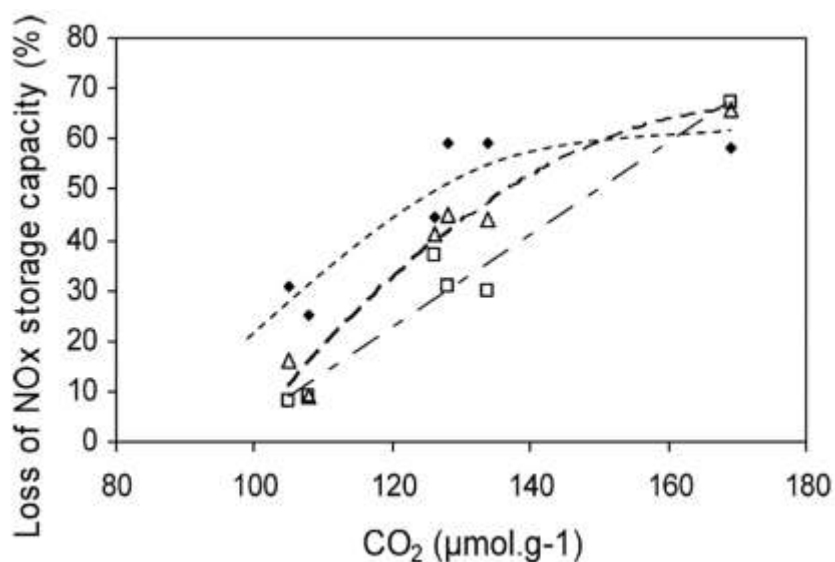


Figure 10: Loss of the NO_x storage capacity (%) due to the presence of CO₂ in the feed gas as a function of the basicity of the catalysts; (□) 200°C, (△) 300°C, (◆) 400°C.

The presence of water in the reaction mixture also induced a more or less harmful effect on NO_x storage depending on catalyst formulation and reaction temperature (Table 7). Table 6 shows that contrarily to CO₂, H₂O affects the NO oxidation activity, in accordance with the literature [25,27,29-31]. However, there is no direct correlation between the loss of NO_x storage capacity and the loss of oxidation activity for the different materials. For alumina containing samples the presence of water in the feed modifies the number of surface hydroxyl groups and therefore the acid-base properties of the oxide support. In a previous work it was shown that adding water to the flow caused the migration of nitrate species from alumina support to barium sites leading to a negligible NO_x adsorption on Al₂O₃ sites [29] in accordance with other papers [9,25,27]. Otherwise water modifies the nature of Ba species on the catalyst surface. Indeed, a part of the BaO sites formed during the pre-treatment at 550°C in the absence of CO₂ and H₂O are transformed into Ba(OH)₂ in the presence of water, leading to less active Ba species for NO_x storage [6,16]. Moreover, for cerium containing catalysts, it has been shown that Ba cerates formed at high temperature decompose under NO₂/H₂O atmosphere around 300°C, contrary to Ba aluminates [37]. The low inhibiting effect of water on the NO_x performance of the Pt/10Ba/CeZr catalyst may thus be attributed to the partial decomposition of these inactive cerates into active Ba species. These different effects of water addition on catalyst properties can explain the more or less significant loss of NO_x storage capacity observed depending on catalyst composition.

Table 8: NO_x storage capacities of catalysts as function of temperature in the presence of CO₂ or CO₂ and H₂O

Catalyst /T(°C)	With CO ₂			With CO ₂ and H ₂ O		
	200	300	400	200	300	400
Pt/10Ba/Al	24.1	22.8	18.0	13.1	13.7	18.3
Pt/20Ba/Al	25.9	24.0	20.4	15.1	16.1	19.2
Pt/20Ba/Al5.5Si	30.2	28.5	17.7	20.0	26.5	22.0
Pt/30Ba/Al5.5Si	22.3	20.4	17.8	14.3	18.6	20.8
Pt/5Ba/CeZr	18.0	18.1	22.0	8.9	12.1	20.0
Pt/10Ba/CeZr	8.7	12.1	23.0	9.4	11.6	22.7
Pt/20Ba/Si	-	-	8.0	3.2	4.2	4.7

Presence of both CO₂ and H₂O

The data obtained with both CO₂ and H₂O in the gas feed are also reported in Table 8. It appears that at 400°C the loss of NO_x storage capacity in the presence of both CO₂ and H₂O is quite similar to that observed with CO₂ alone, except for the Pt/20Ba/Al5.5Si catalyst (Table 7). In this latter case, the effect of CO₂ and H₂O is less harmful than the effect of CO₂ alone, i.e. water would decrease the inhibiting effect of CO₂ on catalyst performances. It is possible that water, which has no direct effect on the NO_x storage capacity of this catalyst at 400°C, modifies the competition between CO₂ and NO_x for adsorption on the Ba component leading to a higher NO_x trapping. Otherwise, Table 7 shows that at lower temperature, i.e. 200°C and 300°C, the simultaneous presence of CO₂ and H₂O induces generally a higher harmful effect than CO₂ or water alone. Only Pt/10Ba/CeZr exhibits the same performances when CO₂ or both CO₂ and H₂O are present in the feed. As water has practically no effect on the storage capacity of this catalyst at 200°C and 300°C, it means that water does not modify the competition of adsorption between CO₂ and NO_x for the storage sites on the catalyst.

The higher inhibiting effect generally observed when both CO₂ and H₂O are present in the feed can be explained by a cumulative effect of CO₂ and H₂O since the two components exhibit a harmful effect when they are introduced separately. As previously discussed, water inhibits the oxidation of NO to NO₂ and the adsorption of NO_x on the support oxide (alumina) while CO₂ competes with NO_x for the adsorption on the basic sites of higher strength (Ba component). Moreover, the presence of water modifies the basic properties of the Ba compound.

Finally, under realistic conditions, with CO₂ and H₂O in the feed gas, Table 8 shows that the best NO_x storage capacities in the whole 200-400°C temperature range were obtained with the Pt/20Ba/Al5.5Si catalyst, i.e. with a material of low surface basicity which limits the competitive

adsorption of CO₂. This result is in accordance with the work of Eguchi and Kikuyama [24,44] on Pt-ZrO₂/Al₂O₃ systems for NO_x trapping. Zirconia was found to possess basicity weak enough to form stable nitrates whereas the carbonate was not produced.

4. Conclusion

The influence of the support oxide (Al₂O₃, SiO₂, Al₂O₃-5.5 wt % SiO₂ and Ce_{0.7}Zr_{0.3}O₂) as well as the Ba loading was studied with regard to the Ba properties towards the rapid NO_x trapping in the presence/absence of H₂O and CO₂. Catalysts were annealed at 700°C in wet oxidizing atmosphere. Crystallized BaCO₃ was detected on all catalysts even at low Ba loading except for Al_{5.5}Si supported samples where it was observed only for the higher Ba loading, indicating a better Ba dispersion on this support. The surface basicity of the catalysts was influenced by both the support oxide and the Ba loading increasing following the order: Pt/20Ba/Si < Pt/20Ba/Al_{5.5}Si < Pt/10Ba/Al < Pt/5Ba/CeZr < Pt/30Ba/Al_{5.5}Si < Pt/20Ba/Al < Pt/10BaCeZr. At 400°C, NO_x storage in the absence of CO₂ and H₂O rose with the material basicity. The optimal storage temperature also increased with the material basicity due to higher nitrate stability.

CO₂ addition in the inlet gas led to a significant decrease of the NO_x storage capacity for all the catalysts. The CO₂ inhibiting effect grew with both the basicity of the catalysts and the storage temperature. H₂O had a less negative effect than CO₂ on the NO_x storage capacity, alumina containing materials being more affected than ceria-zirconia supported samples. When both CO₂ and H₂O were present in the inlet gas, a cumulative effect was observed at low temperatures (200°C and 300°C) while mainly CO₂ was responsible for the loss of the NO_x storage capacity at 400°C.

In the whole 200-400°C temperature range under realistic conditions (CO₂, H₂O), the Pt/20Ba/Al_{5.5}Si catalyst showed the best performances for the rapid NO_x uptake. It resulted mainly from enhanced dispersions of platinum and barium on the alumina-silica support, a high Pt-Ba proximity and a low basicity of the catalyst which limits the CO₂ competition for the storage sites.

Acknowledgments

This work was financially supported by the French Environment and Energy Management Agency (ADEME) and the Poitou-Charentes Region.

References

- [1] N. Miyoshi, S. Matsumoto, K. Katoh, J. Harada, N. Takahashi, K. Yokota, M. Sugiura, K. Kasahara, SAE Tech. Paper 950809, 1995.
- [2] W.S. Epling, L.E. Campbell, A. Yezerets, N.W. Currier, J.E. Parks II, Catal. Rev. 46 (2004) 163.
- [3] P.J. Schmitz, R.J. Baird, J. Phys. Chem B 106 (2002) 4172.
- [4] H. Mahzoul, J.F. Brilhac, P. Gilot, Appl. Catal. B: 20 (1999) 47.
- [5] K.S. Kabin, P. Khanna, R.L. Muncrief, V. Medhekar, M.P. Harold, Catal. Today 114 (2006) 72.
- [6] L. Lietti, P. Forzatti, I. Nova, E. Tronconi, J. Catal 204 (2001) 175.
- [7] F. Rodrigues, L. Juste, C. Potvin, F.F. Tempere, G. Blanchard, G. Djega-Mariadassou, Catal. Lett. 72 (2001) 59.
- [8] N.W. Cant, M.J. Patterson, Catal. Today 73 (2002) 271.
- [9] W.S. Epling, J.E. Parks, G.C. Campbell, A. Yezerets, N.W. Currier, L.E. Campbell, Catal. Today 96 (2004) 21.
- [10] E. Fridell, H. Persson, L. Olsson, B. Westerberg, A. Amberntsson, M. Skoglundh, Top. Catal 16/17 (2001) 133.
- [11] P. Broqvist, I. Panas, E. Fridell, H. Persson, J. Phys. Chem B 106 (2002) 137.
- [12] L. Olsson, H. Persson, E. Fridell, M. Skoglundh, B. Andersson, J. Phys. Chem. B 105 (2001) 6895.
- [13] M. Piacentini, M. Maciejewski, A. Baiker, Appl. Catal. B 60 (2005) 265.
- [14] C.M.L. Scholz, V.R. Gangwal, M.H.J.M. de Croon, J.C. Schouten, J. Catal 245 (2007) 215.
- [15] N.W. Cant, I.O.Y. Liu, M.J. Patterson, J. Catal 243 (2006) 309.
- [16] T. Kobayashi, T. Yamada, K. Kayano, SAE Tech. Paper 970745 (1997).
- [17] M. Piacentini, M. Maciejewski, A. Baiker, Appl. Catal. B 66 (2006) 126.
- [18] P. Svedberg, E. Jobson, S. Erkfeldt, B. Andersson, M. Larsson, M. Skoglundh, Top. Catal., 30/31 (2004) 199.
- [19] S. Philip, A. Drochner, J. Kunert, H. Vogel, J. Theis, E.S. Lox, Top. Catal., 30, (2004) 235. [20] L.F. Liotta, A. Macaluso, G.E. Arena, M. Livi, G. Centi, G. Deganello, Catal. Today, 75 (2002) 439.
- [21] E.C. Corbos, S. Elbouazzaoui, X. Courtois, N. Bion, P. Marecot, D. Duprez, Top. Catal. 42/43 (2007) 9.
- [22] M. Waqif, A. Pieplu, O. Saur, K.C. Lavalley, G. Blanchard, Solid State Ionics, 95 (1997) 163.
- [23] S.M. Mathew, S.B. Umbarkar, M.K. Dongare, Catal. Comm. 8 (2007) 1178.
- [24] K. Eguchi, T. Kondo, T. Hayashi, H. Arai, Appl. Catal. B 16 (1998) 69.
- [25] C.M.L. Scholz, V.R. Gangwal, J.H.B.J. Hoebink, J.C. Schouten, Appl. Catal. B: 71 (2007) 143.
- [26] I. Nova, L. Castoldi, L. Lietti, E. Tronconi, P. Forzatti, Catal. Today 2747 (2002) 1.
- [27] A. Lindholm, N.W. Currier, E. Fridell, A. Yezerets, L. Olsson, Appl. Catal. B (2007) accepted manuscript.
- [28] S. Balcon, C. Potvin, L. Salin, J.F. Tempère, G. Djega-Mariadassou, Catal. Lett., 60 (1999) 39. [29] T. Toops, D.B. Smith, W.S. Epling, J.E. Parks, W.P. Partridge, Appl. Catal. B: Environ., 58 (2005) 255.
- [30] L. Olsson, M. Abul-Milh, H. Karlsson, E. Jobson, P. Thormaehlen, A. Hinz, Top. Catal., 30/31 (2004) 85.
- [31] S.S. Mula, N. Chen, L. Cumaranatunge, W.N. Delgass, W.S. Epling, F.H. Riberio, Catal. Today, 114 (2006) 57.
- [32] Y. Madier, PhD. Thesis, Poitiers University (1999).
- [33] S.J. Gregg, K.S.W. Sing, "Adsorption, Surface Area and Porosity", Academic Press London and New York (1967).
- [34] G.W. Graham, H.W. Jen, J.R. Theis, R.W. McCabe, Catal. Lett 93 (2004) 3.
- [35] T. Szailer, J.H. Kwak, D.H. Kim, J. Szanyi, C. Wang, C.H.F. Peden, Catal. Today 114 (2006) 86.
- [36] M. Eberhardt, R. Riedel, U. Gobel, J. Theis, E.S. Lox, Top. Catal. 30/31 (2004) 135.
- [37] M. Casapu, J.D. Grunwaldt, M. Maciejewski, M. Wittrock, U. Gobel, A. Baiker, Appl. Catal. B 63 (2006) 232.
- [38] C.T. Au, H. He, S.J. Lai, C.F. Ng, Appl. Catal. A 159 (1997) 133.
- [39] W.S. Epling, G. Campbell, J. Parks, Catal. Lett. 90 (2003) 45.
- [40] E. Fridell, H. Persson, B. Westerberg, L. Olsson, M. Skoglundh, Catal. Lett. 66 (2000) 71.

- [41] Y. Li, S. Roth, J. Dettling, T. Beutel, *Top. Catal.* 16/17 (2001) 139.
- [42] B. Westerberg, E. Fridell, *J. Molec. Catal. A: Chemical* 165 (2001) 139.
- [43] L. Olsson, E. Fridell, *J. Catal* 210 (2002) 340.
- [44] S. Kikuyama, I. Matsukuma, R. Kikuchi, K. Sasaki, K. Eguchi, *Appl. Catal. A* 226 (2002) 23.